ERJ
Engineering Research Journal
Faculty of Engineering
Minoufiya University

BEHAVIOR OF DIESEL FUEL INJECTION SYSTEM WHEN RUNNING WITH BIODIESEL

Safwat A. Wilson

Mechanical Power Engineering Department, Faculty of Engineering, Minoufiya University, Shebin El-Kom, Egypt

ABSTRACT

The study aims to approach the performance of fuel injection system of diesel engines when using biodiesel as an alternative fuel. Mathematical model is proposed to simulate the fuel path through the injection system taking into consideration the compressibility effect, pressure waves in the pipeline, fuel properties and the leakage through clearance of moving parts. The model is compared with another experimental work for validation. The effect of biodiesel properties and its blends on the injection system behavior are examined. The results indicate that, when using biodiesel as an alternative fuel, the pressure waves propagating through the line diminished rapidly compared with conventional diesel oil. The results indicate also that, when using biodiesel, the leakage decreased because of its higher viscosity. As a result, the rate of pressure rise increases and the beginning of injection becomes earlier. It is important in this case to retard the injection timing to optimize the engine performance. On the other hand, the study shows that, the same atomization degree can be obtained when transformed to biodiesel by raising the injection pressure with certain ratios. These ratios depend on biodiesel blend percentage and compression ratio of the engine.

يقدم البحث الحالى دراسة عن تأثير استخدام الوقود الحيوى على أداء منظومات الحقن فى محركات الديزل. فى هذا الإطار تم اقتراح نموذج نظرى لتمثيل سريان الوقود خلال منظومة الحقن مع الأخذ فى الاعتبار الحركة الميكانيكية لأجزاء المنظومة وسريان موجات الضغط داخل أنبوبة الحقن وتأثير الانضغاطية على سلوك الوقود داخل المنظومة. كما تم فى البحث الحالى إدخال تأثير الوقود المنساب بين خلوص الأجزاء المتحركة. وقد أوضحت الدراسة الحالية أن لزوجة الوقود الحيوى تساعد على إخماد موجات الضغط داخل الأنابيب بعد انتهاء الحقن مما يقلل من احتمالية حدوث حقن متتالٍ أو تسييل من فوهة الوقود. إلا أن كمية الوقود المنسابة خلال الأجزاء المتحركة قد انخفضت بسبب ارتفاع اللزوجة، الأمر الذى ساهم بالإضافة الى خصائص الوقود فى رفع معدل تغير الضغط داخل المنظومة مما أدى الى تبكير بدء الحقن بالمقارنة باستخدام وقود الديزل مما يحتم تعديل توقيت نظام الحقن للحصول على الأداء الأمثل. كما أوضحت الدراسة أنه يمكن الوصول إلى نفس مستوى التذرير الناتج عن وقود الديزل وذلك برفع ضغط الحقن بنسب تعتمد على كل من نسبة الوقود الحيوى الى وقود الديزل وكذلك نسبة الانضغاط.

Keywords: Fuel injection system, biodiesel, mathematical model, compression ignition engines.

1. INTRODUCTION

During the last decade, several attempts were made to produce multi fuel engines. Attention were focused on using non-fossil fuel in diesel engines. Vegetarian base oil is proposed as a suitable alternative fuel[1]. As the viscosity, surface tension and density of the raw vegetable oil is higher than that of diesel oil, the atomization process is somewhat poor and the resultant droplets become bigger. This increases the probability of unburned hydrocarbons in the exhaust products. Engines run with neat vegetable oils are equipped with preheaters in order to reduce the oil viscosity to a suitable value[2-4]. On the other hand, combustion of bigger hydrocarbon compounds in vegetable oil leads to undesired components like gum resin, which causes piston ring sticking. For this reasons, alkyl esters were extracted from the vegetable oils by removing glycerin. The resultant is a fuel having physical properties more suitable for diesel engine called biodiesel oil. The term biodiesel represents a wide range of hydrocarbon compounds differing from each other according to their vegetarian origin and the extracting process [5,6]. Biodiesel can be extracted from edible oils like coconut, palm, olive, soybeans, sunflower, maize and seeds of some other plants [7-

16]. Non-edible oils are also important source of biodiesel like jojoba, karanja, jatropha and others[17-23]. In spite of some differences in chemical structure, all types of biodiesel contain oxygen, which contributes to lower the heating value. The other common factor is their negligible content of sulfur which means more clean exhaust gases from sulfur compounds. The other significant advantage of using biodiesel as a fuel appears in its high lubricity, which reflects on reducing wear in mechanical parts of engines and increasing its durability [24-26].

Behaviors of diesel engines when running with biodiesel were addressed [27-35]. The engines performance and their emission were studied extensively to clear the effect of fuel factor. The previous works indicate that, cleaner exhaust can be achieved when using biodiesel as neat oil or as blend with diesel oil without scarifying the performance[36-38]. ASTM and engine manufacturer association *EMA* recommended to use blends of 20% biodiesel with 80% diesel oil known as B20 [39]. This blend can be used without any modification on engines, and the performance is rarely affected. National biodiesel board indicated that, in spite of promising results of higher blend ratio, there is some precautions that must be considered [40]. Biodiesel blends higher than B20 can cause problems with natural rubber engine components, such as seals and hoses. On the other hand, economical studies [41] indicate that biodiesel is competitive with CNG and methanol fuels but it less competitive compared with petroleum diesel fuel. With rising petroleum prices, biodiesel becoming more economically competitive.

The present work aims to highlight fuel system performance when it works with biodiesel oil. The study is based on developing mathematical model derived from its original version [42]. The rate of pressure rise, wave propagation through pipeline and the probability of after injection were addressed. The present model considered the leakage of fuel through the clearance of moving parts as well as the dynamic representation of cam follower mechanism. The importance of leakage comes from the fact that great amount reduces the fuel injected and collapses the injection pressure, but on the other hand, the little amount of leakage is important for lubricity. So the study contributes to clear the factors affecting such leakage and helps to adapt its value in order to obtain better injection parameters.

2. MATHEMATICAL MODEL

The fuel injection system in diesel engines consists mainly of three parts. The high-pressure pump, delivery pipe and injector are the most important components of the injection system. These parts are linked together mechanically and hydraulically. The complete model simulates the flow path since the fuel enters the high pressure pump until leaving the injector taking into consideration the compressibility effect of the fuel, pressure waves traveling through the delivery pipe and the fuel leakage through the clearance between moving parts. The kinematics of cam plunger system is included also as well as the motion of delivery valve and needle valve. The typical fuel system considered in the present work is represented in Fig. 1. In the following, the complete description of the present mathematical model is introduced.

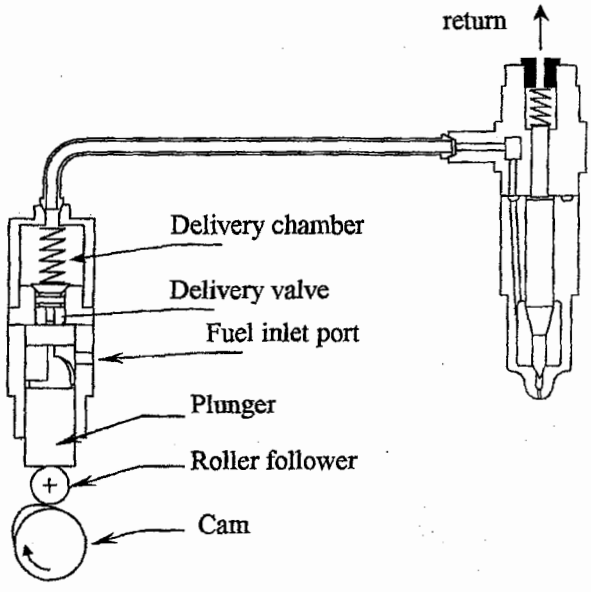

Fig. 1 Fuel injection system used in present model

Pump side

The proposed mathematical model begins with the cam-follower mechanism [43]. The instantaneous lift of roller follower with respect to the rotation of cam is illustrated in Fig. 2. As the cam rotates, the follower becomes in contact with tangent flank and the instantaneous lift is given as follows.

$$l = \left(R + R_b\right)\left(\frac{1}{\cos\theta} - 1\right) \tag{1}$$

During this period, the follower increases its velocity with certain acceleration. Further rotation of cam puts the follower in contact with cam nose, and the instantaneous follower lift is obtained as follows.

$$l = \left(\sqrt{\left(R + r_n\right)^2 - D^2 \sin^2\gamma}\right) + D\cos\gamma - \left(R + R_b\right) \tag{2}$$

where,

$\gamma = \phi - \theta$

and,

$$D = \frac{R_b - r_n}{\cos\phi}$$

The cam angle at which the follower leaves the tangent flank and becomes in contact with nose circle is assigned as follows.

$$\theta_m = tan^{-1}\left[tan\phi\left(1-\frac{r_n+R}{R_b+R}\right)\right] \quad (3)$$

During this period, the follower continues its motion but with deceleration until it reaches the maximum lift. The linear follower velocity and its acceleration is obtained as follows.

Follower velocity:

$$u_p = \frac{dl}{dt} = \varpi\frac{dl}{d\theta} \quad (4)$$

Follower acceleration :

$$a_p = \frac{du_p}{dt} = \varpi^2\frac{d^2l}{d\theta^2} \quad (5)$$

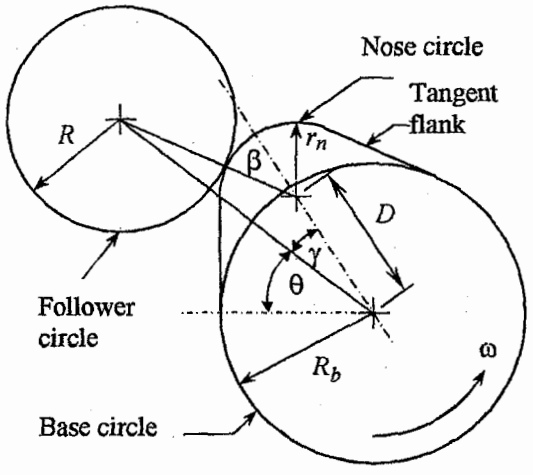

Fig. 2 Cam-follower mechanism

The instantaneous follower/plunger lift and its velocity are represented in dimensionless form as shown in Fig. 3. It is clear from the figure that, the velocity increases when the follower is in contact with flank until it reaches its maximum velocity at the end of this period. During nose contact period, the follower decreases its velocity until it reaches the maximum lift.

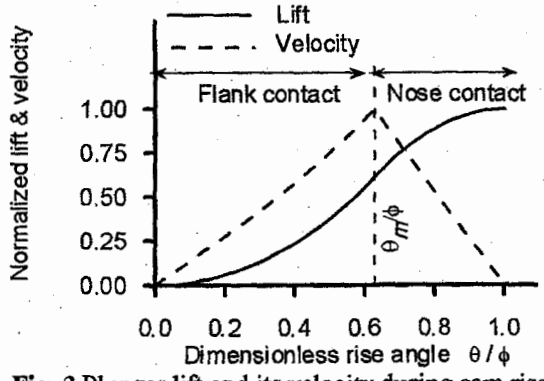

Fig. 3 Plunger lift and its velocity during cam rise period

Deviation between cam profile and follower/plunger lift is indicated in Fig.4. Deviation comes from the shift between the contact point and follower/plunger axis. This difference depends on the ratio between follower radius and base circle radius

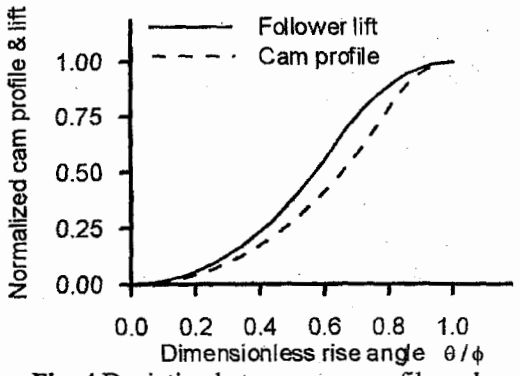

Fig. 4 Deviation between cam profile and follower lift

Assigning the flow path through the pump barrel requires the solution of continuity equation as follows. As the plunger proceeds in compression stroke, the resultant displacement volume distributes to different sites as shown in Fig. 5. When the delivery valve opens the fuel flows to delivery chamber, the other amount of fuel returns to the inlet port if it is still open. Besides, small amount of fuel leaks through plunger clearance. The rest represents the amount of fuel compressed inside the pump barrel, which appears as a change in fuel pressure. This is expressed mathematically as follows

$$A_p u_p + Q_{in} - Q_d - Q_l = \left(\frac{dV_p}{dt}\right) \quad (6)$$

Each term of the last equation is defined individually as follows.

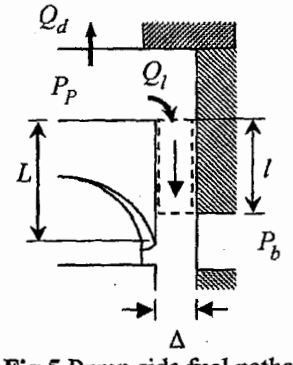

Fig.5 Pump side fuel paths

Plunger displacement

$$A_p u_p = \frac{\pi}{4}d_p^2\frac{dl}{dt} = \varpi\frac{\pi}{4}d_p^2\frac{dl}{d\theta} \quad (7)$$

Fuel inlet/outlet flow rate Q_{in}

$$Q_{in} = C_d A_{in} \left(P_o - P_p\right) \frac{\sqrt{2\rho}}{\sqrt{\left|P_o - P_p\right|}} \tag{8}$$

Inlet port timing and its effective area are illustrated in Figs. 6 and 7, respectively. The variation of inlet port area is incorporated in present model where,

$$A_{in} = f\left(d_{in}\ ,\ \alpha\ ,\ L_{st}\ ,\ \theta\right) \tag{9}$$

It is clear from the last function that, instantaneous inlet port area depends on inlet port diameter, angle of helical groove α, effective stroke L_{st} and plunger displacement, which in turn depends on the cam profile and angle of rotation θ. The effective stroke appears clearly in Fig. 7. as the period at which the inlet port area becomes zero.

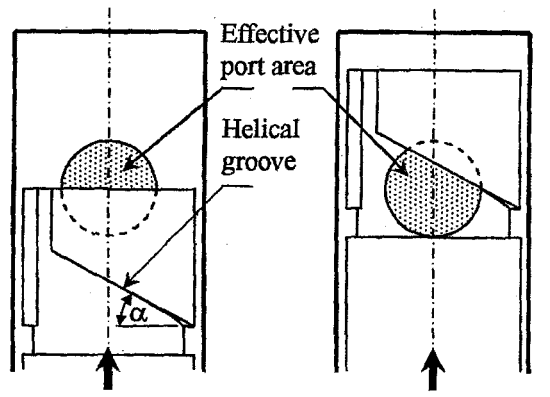

(a) Before injection (b) After injection

Fig. 6 Variation of inlet port area during plunger movement

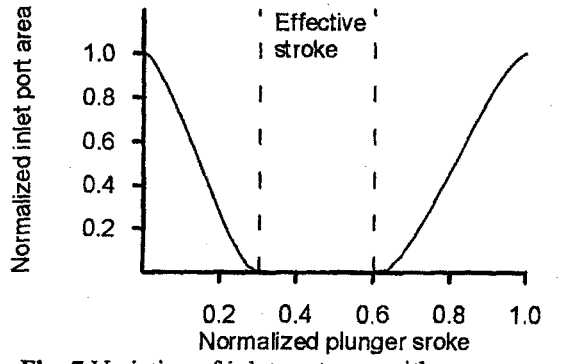

Fig. 7 Variation of inlet port area with respect to plunger stroke

Fuel delivered to delivery chamber Q_d

When the delivery valve exposed to pressure difference exceeding the initial tightening force, it begins to move. This motion causes suction in pump side and compression in delivery chamber side until it reaches a certain height called relief stroke. Further motion leads to open the valve and permit the fuel to discharge into delivery chamber. This process is reversed at the end of injection to ensure fast closing for injector valve.

So, if $x < x_r$

$$Q_d = A_d \frac{dx}{dt} \tag{10}$$

If $x > x_r$

$$Q_d = C_d A_d \left(P_p - P_d\right) \frac{\sqrt{2\rho}}{\sqrt{\left|P_p - P_d\right|}} \tag{11}$$

Rate of change in fuel volume

Considering the fuel as elastic material, the relation between stress exerted on control volume and corresponding strain is as follows.

$$dP = E \frac{dV}{V} \tag{12}$$

where, E is the modulus of elasticity for fuel. So, the rate of fuel change is expressed as follows.

$$\frac{dV_p}{dt} = \frac{V}{E} \frac{dP_p}{dt} \tag{13}$$

Substituting rate of change in fuel volume into Eq.(6) the corresponding rate of pressure rise inside pump barrel is obtained.

Delivery chamber side

Total change in fuel volume inside delivery chamber comes from the discharged volume from pump side or displacement caused by delivery valve and the outflow through the pipeline as shown in Fig. 8. The sum of these terms is equal to the change in fuel volume inside the delivery chamber, which reflects on a change in pressure.

$$\frac{dV_d}{dt} = Q_d - Q_{pipe} \tag{14}$$

The last equation is used to calculate the change in delivery chamber pressure considering the elasticity in fuel as follows.

$$\frac{dP_d}{dt} = \frac{E}{V_d} \left(Q_d - Q_{pipe}\right) \tag{15}$$

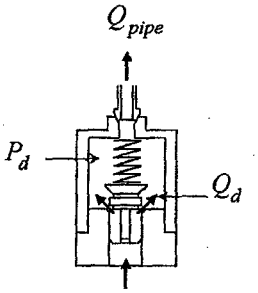

Fig. 8 Delivery chamber

In order to calculate the value of Q_d as represented in Equations (10) and (11), the valve motion must be assigned. Considering frictionless motion, the effective forces acting on the valve are illustrated in Fig. 9. Accordingly, the equation of motion is then as follows:

$$m_d \frac{d^2x}{dt^2} = \left(P_p - P_d\right) A_d - k_d \left(x + x_o\right) \tag{16}$$

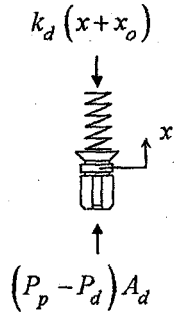

Fig. 9 Forces exerted on delivery valve

Delivery pipe

The flow of fuel through the pipeline is treated as one-dimensional, time dependent flow. The compressibility of fuel is considered also. Temporal pressure and velocity distribution along the pipeline is obtained by employing continuity and momentum equation as follows:

Continuity

$$\frac{\partial \rho}{\partial t} + \rho \frac{\partial u}{\partial x} = 0 \tag{17}$$

Momentum

$$\rho \frac{\partial u}{\partial t} + \rho u \frac{\partial u}{\partial x} = -\frac{\partial P}{\partial x} + \mu \frac{\partial^2 u}{\partial x^2} \tag{18}$$

The previous differential equations are solved together numerically via control volume method. The staggered grid is used in present mathematical treatment as illustrated in Fig. 10. This grid style is more convenient for integrating continuity equation. In this technique, two separate groups of cells are used for continuity and momentum equations respectively. The two groups have an overlap structure as shown in Fig.10. The grid size Δx is the same for both types of cells and it must be defined precisely for good representation of pressure wave propagation and to satisfy the criterion of numerical stability. This can be achieved when Courant number becomes less than unity [44] as follows.

$$C = \left(|u| + a\right)\frac{\Delta t}{\Delta x} < 1 \tag{19}$$

The residual pressure inside the pipeline is considered as initial condition for the flow through pipeline, while the pressure and fuel velocity at the delivery chamber and injector are considered as boundary conditions at each time step.

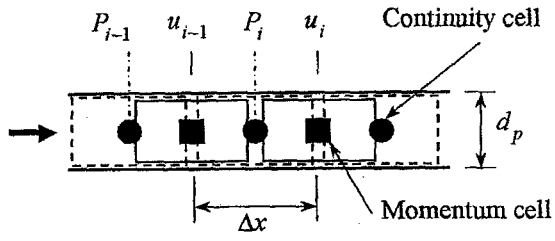

Fig.10 Grid used in numerical treatment for flow through pipeline

Injector side

The quantity of fuel entering and leaving the needle chamber as well as the leakage through the gap between needle and its bush controls the rate of pressure change inside the injector as shown in Fig. 11. Also, the displacement volume due to needle valve motion causes a significant temporal change in the volume inside the needle chamber during its motion. Finally, the net change in volume inside needle chamber is calculated as follows:

$$\frac{dV_n}{dt} = Q_{in} - Q_{inj} - Q_l - Q_n \tag{20}$$

From the last equation, the rate of change of pressure inside the needle chamber is obtained considering the compressibility effect as follows:

$$\frac{dP}{dt} = \frac{V_n}{E}\left(Q_{in} - Q_{inj} - Q_l - Q_n\right) \tag{21}$$

where,

$Q_{in} = A_{pipe} u_{in}$

u_{in} is the inlet fuel velocity to needle camber passage and is considered as the exit fuel velocity from pipeline. The volume flow rate of fuel injected depends on both the injector and back pressures, respectively, as follows:

$$Q_{inj} = A_{eff}\left(P_n - P_b\right)\frac{\sqrt{2\rho}}{\sqrt{|P_n - P_b|}} \tag{22}$$

where, A_{eff} is the effective area at which the fuel is injected, and its value is obtained as represented in Appendix A.

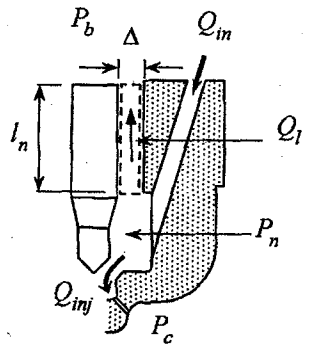

Fig.11 Fuel paths through injector

The displacement volume caused by the needle valve motion is calculated as follows:

$$Q_n = \frac{\pi}{4} d_n^2 . \frac{dy}{dt} \tag{23}$$

As appears in Equations (A.2) and (23), the assignment of instantaneous needle valve lift 'y' is essential. Its value is obtained by analyzing the effective forces acting on the needle and considering frictionless motion as shown in Fig. 12.

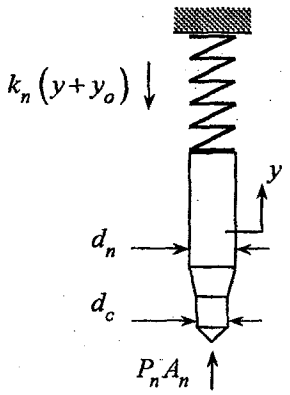

Fig. 12 Force balance for needle valve

It is important to mention that, before the first wave front reaches the needle chamber, the needle is in contact with its seat. In this case, the fuel pressure affects the upper frustum only. When the needle is set to move, the pressure affects the full cross section area of the needle. Accordingly, equation of the needle valve motion is calculated as follows:

$$m_n \frac{d^2 y}{dt^2} = P_n A_n - k_n (y + y_o) \tag{24}$$

When $y = 0$

$$A_n = \frac{\pi}{4}\left(d_n^2 - d_c^2\right) \tag{25}$$

At $y > 0$

$$A_n = \frac{\pi}{4} d_n^2 \tag{26}$$

Leakage treatment

During the active compression stroke and due to the steady increase in pressure in confined space, fuel finds its way to leak between the clearance of moving parts. The leakage is confined in two sites inside the fuel system. In the first location, back flow of fuel through plunger/bush clearance to feeding port is considered. The other leakage of fuel occurs through the clearance between injector needle and injector body. Figures 5 and 11 show the path of leakage fuel through the clearance of moving parts. When the gap is small (5 μm on average), the flow of fuel is considered as laminar, one-dimensional and incompressible. According to these assumptions, the volume flow rate of leak fuel becomes [45]:

$$Q_l = \frac{\Delta P}{12\mu} \Delta^3 \frac{\pi d}{l} \tag{27}$$

Where, ΔP represents the difference between upstream and downstream pressure, d is the plunger or needle diameter. The last relation is driven for still plunger/ bush clearance. In case of leakage between moving parts, the relative fluid velocity must be taken into consideration. While Reynolds number of back flow or leakage is very low, the flow is considered as Couette flow at which the velocity is linearly distributed across the gap due to the plunger motion. For no slip condition fluid adjacent bush wall has zero velocity and at plunger surface it takes its velocity. Accordingly, the last equation becomes.

$$Q_l = \left(\frac{\Delta P}{12\mu} \frac{\Delta^2}{l} \pm \frac{1}{2} u_P \right) \pi d \Delta \tag{28}$$

where, u_P is the plunger/needle velocity. Velocity sign indicates the flow direction relative to the moving parts. Total amount of fuel leaks through the clearance of both plunger/bush and needle/bush is obtained by integrating previous equations with respect to time as follows:

$$Q_{l(total)} = \int (Q_l)_{plunger} dt + \int (Q_l)_{needle} dt \tag{29}$$

The relative fuel leakage per active stroke is assigned as follows:

$$q_l)_{tot} = \frac{(Q_l)_{total}}{(\pi/4) d_p^2 l_{st}} \tag{30}$$

Cavitation treatment

Under some circumstances, especially at the end of injection, the fuel pressure falls to the vapor pressure. This physically means cavitaion occurrence, which appears in calculations as negative pressure. So at any control volume in the system that experiences such phenomenon, the pressure is considered as

vapor pressure and the resultant void volume is calculated as follows:

$P < P_v$ then,

$$P = P_v \tag{31-a}$$

and,

$$\frac{dV_{void}}{dt} = Q_{in} - Q_{out} \tag{31-b}$$

Pipeline residual pressure

By the end of each injection cycle, both the injector needle and delivery valve were closed. The pressure waves propagating through the pipeline are then reflected from one side to another until it settles at certain level called residual pressure. The present model presumes the residual pressure inside the pipeline. After each cycle of calculation, this value is recalculated and compared with previous one. If the difference exceeds the allowable limit, new cycle of calculation is performed with updated value until convergence is reached. The value of residual pressure is calculated according to the following principle. The sum of the compressed volume inside each pipeline element is equal to the total compressed volume inside the whole pipeline. This can be expressed mathematically as follows:

$$\Delta V_{tot} = \frac{V_{pipe}}{E} P_{rez} = \sum_{i=1}^{i=n} \frac{V_i}{E} P_i \tag{32}$$

While volume of each pipeline element 'V_i' and modulus of elasticity E are considered constant (because at the end of each injection cycle, the pressure fluctuations inside pipe line becomes small), then for constant pipe cross section area the residual pressure is calculated as follows:

$$P_{rez} = \frac{\Delta x}{L_{pipe}} \sum_{i=1}^{i=n} P_i \tag{33}$$

3. MODEL VALIDATION

Output results of the present model are compared with experimental data [46] to validate the present model. Instantaneous rate of fuel injection, needle valve motion and cumulative amount of fuel injected were considered as shown in Fig (13). Comparison shows fair agreement in spite of small angular shift. The present model shows early opening in needle valve and consequently early closing, this may be due to differences in cam profile simulation. The rate of needle valve motion in present model is somewhat slow and this reflects on increasing the injection pressure during such period compared with recorded data which appears as higher rate of fuel injection as shown in Figure 13-b. The same result is obtained when comparing the cumulative fuel during the injection stroke as shown in Fig. 14.

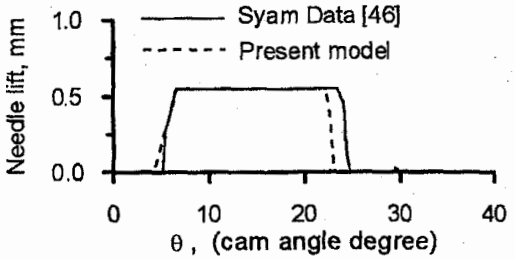

Fig. 13-a Needle valve motion

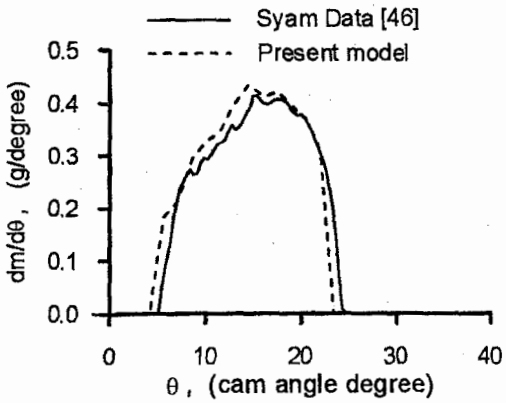

Fig. 13-b Comparison between Syam data [46] and present model

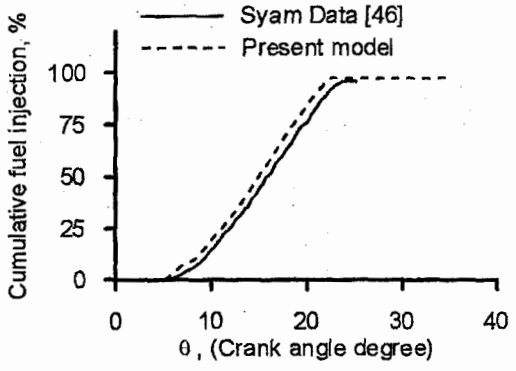

Fig. 14 Cumulative fuel injection during injection stroke

4. RESULTS AND DISCUSSION

Because of its great availability and possessing high content of methyl ester in its composition [47], soy methyl ester is considered as biodiesel in the preset study. The properties of neat biodiesel (B100) and its blend with diesel fuel are examined with the present model in order to address their effect on the fuel injection system performance.

4.1 Fuel properties

Physical and chemical properties for biodiesel, diesel fuel and blends were obtained experimentally

[48,49]. Density was found to be linearly dependent on pressure, temperature and blend ratio. Experimental data representing fuel density is correlated as in the following form [48].

$$\rho = a_1 T + a_2 P + a_3 B + a_4 \quad (34)$$

The values of regression constants are given in Table (1).

Table 1 Density regression constants [48]

Coefficients	Biodiesel with No. 2 diesel fuel blend	Biodiesel with No. 1 diesel fuel blend
$a_1 \times 10^4$	-6.5302	-6.5757
$a_2 \times 10^4$	5.8574	6.1040
$a_3 \times 10^4$	2.6324	5.9030
$a_4 \times 10$	8.6671	8.3318

Speed of sound data was correlated with more three variable polynomials. The correlation includes the nonlinear effect of pressure, temperature and blend ratio on the sonic speed as follows:

$$C = a_1 T + a_2 P + a_3 B + a_4 T.P + a_5 P.B + a_6 P^2 + a_7 B^2 + a_8 \quad (35)$$

where, T in ^oC, P in MPa. and B is a biodiesel percentage. The regression constants for sonic speed are listed in Table (2).

Table 2 Regression constants for sonic speed [48]

Coefficients	Biodiesel with No. 2 diesel fuel blend	Biodiesel with No. 1 diesel fuel blend
a_1	-3.5972	-3.7043
a_2	4.6849	5.0232
$a_3 \times 10$	2.3682	6.5479
$a_4 \times 10^2$	1.4412	1.4958
$a_5 \times 10^3$	-3.9664	-6.9146
$a_6 \times 10^2$	-1.6236	-1.7425
$a_7 \times 10^4$	8.8429	11.8120
$a_8 \times 10^{-3}$	1.4570	1.4147

Bulk modulus is estimated depending on previously obtained density and sonic speed as follows:

$$E = \rho C^2 \quad (36)$$

Viscosity of biodiesl and its blends with diesel fuel No.2 is given in Table (3) [50].

Table 3 Viscosity of diesel fuel and biodiesel blends

Fuel	Diesel	Biodiesel (B100)	B20	B5
Viscosity, cSt. @ 40 °C [50]	3.11	4.75	3.36	
Viscosity, cSt. @ 80 °C [51]	1.4	2.01	1.5	1.43
Surface tension mN/m [51]	25.21	27.15	25.59	25.30
Specific gravity [51]	0.801	0.841	0.809	0.803

Other properties are given in Appendix B.

The fuel properties reported above are used in the present model to examine their effect on injection system characteristics. The standard configuration of the fuel injection system for Deutz F1l511 diesel engine (given in Appendix C) is used in present study. The results show that, the behavior of B20 in fuel system is so far resembled to neat diesel No. 2 (B0). However, net biodiesel (B100) showed significant differences. According to its higher viscosity, B100 shows great tendency to damp the pressure waves propagating in the pipeline after each successive injection as shown in Fig. 15. On the other hand, for the same volumetric change in fuel during the active compression stroke, the higher bulk modulus leads to an increase in the rate of pressure rise. This, in turn, leads to earlier injection timing and higher injection rate as shown in Figs 16 and 17, respectively. While B20 begins early injection by 0.4 crank angle degree relative to diesel No. 2, the neat biodiesel starts the injection 1.2 degree earlier. This means that when using B100 in engines, the injection timing must be retarded by the same value. On the other hand, the early start means longer injection duration, and when considering the relative high injection pressure of B100 the resultant is injecting higher quantity of fuel compared with diesel fuel as shown in Fig 18.

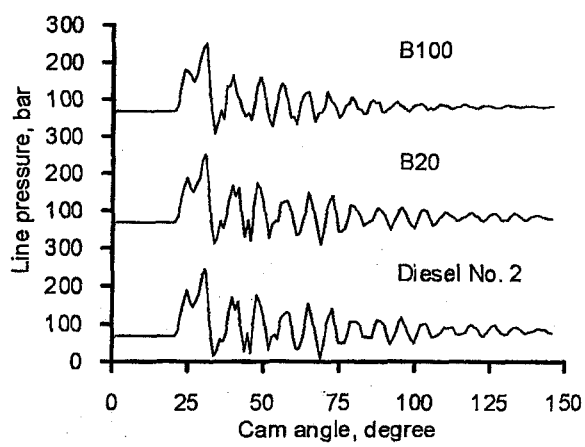

Fig. 15 Variation of line pressure at different fuel types, (engine speed 1500 rpm)

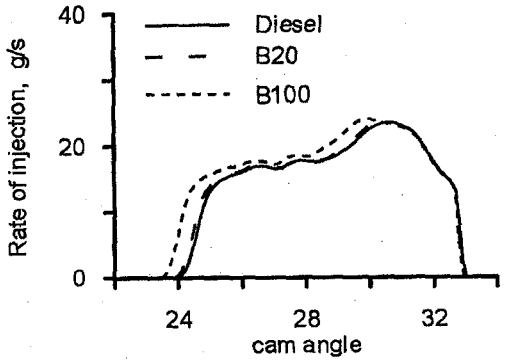

Fig. 16 Rate of fuel injection (engine speed 1500 rpm)

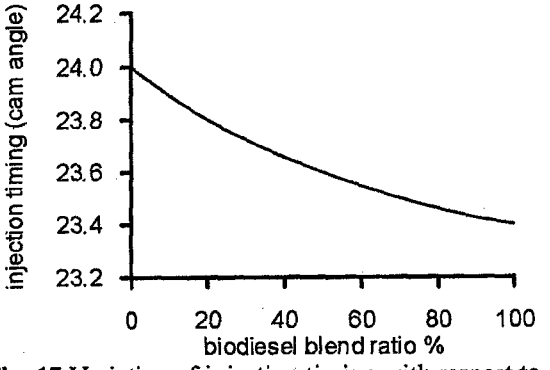

Fig. 17 Variation of injection timing with respect to biodiesel blend ratios, (engine speed 1500 rpm)

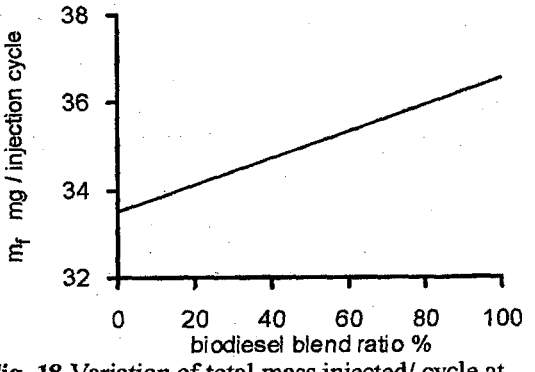

Fig. 18 Variation of total mass injected/ cycle at different biodiesel blends, (engine speed 1500 rpm)

Accordingly, the trapped quantity of fuel inside pipeline decreased in case of using B100. This, in turn, reduces the residual pressure inside the line as shown in Fig. 19. The nonlinearity in this relation comes from multiple fuel properties affecting the residual pressure such as viscosity and bulk modulus.

The viscosity of the fuel plays another role in controlling the fuel backflow to pump feeding port and the leakage through the clearance of needle/injector body. As clear in Equations 27 & 28, the amount of leakage is inversely proportional to the fuel viscosity. So, the higher the viscosity the lower the leakage as shown in Fig. 20.

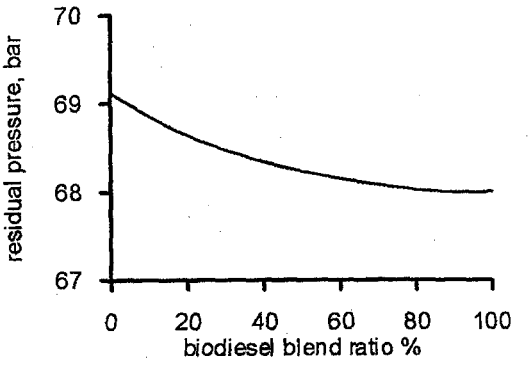

Fig.19 Change in line residual pressure (engine speed 1500 rpm)

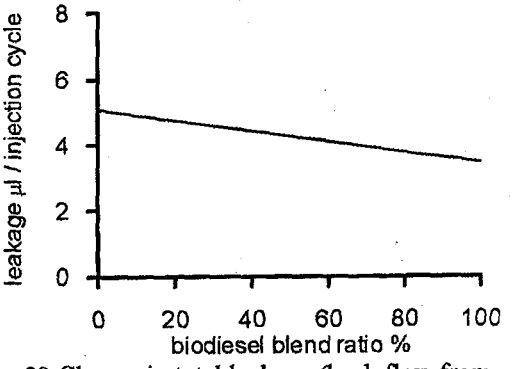

Fig. 20 Change in total leakage (back flow from pump port + leakage through injector needle clearance), (engine speed 1500 rpm)

4.2 Atomization characteristics

The effect of fuel factor on atomization process was addressed. The dependency of resultant Sauter mean diameter D_{32} on the fuel properties and operating condition becomes clear and is represented in the following correlation [51].

$$D_{32} = 6156\ \nu^{0.385}\ \sigma^{0.737}\ \rho^{0.737}\ \rho_a^{0.06}\ \Delta P_L^{-0.54} \tag{37}$$

The previous correlation is used to estimate the operating pressure for fuel system required to obtain the same D_{32} when using the commercial diesel fuel. For the same ambient condition (ρ_a) and D_{32}, the previous correlation can be rearranged in the following form:

$$\frac{(\Delta P_L)_{bio}}{(\Delta P_L)_d} = \left(\frac{\nu_{bio}}{\nu_d}\right)^{0.713} \left(\frac{\sigma_{bio}}{\sigma_d}\right)^{1.365} \left(\frac{\rho_{bio}}{\rho_d}\right)^{1.365} = PR \tag{38}$$

For biodiesel, the increase in injection pressure required to obtain the same D_{32} as in diesel fuel is then derived as follows:

$$\frac{P_{bio}}{P_d} = PR - \frac{P_c(R-1)}{P_d} \quad (39)$$

The previous ratio is called injection pressure ratio. Values of PR depends only on the physical properties of the fuels, so it is calculated for different biodiesel blends (B100, B20 and B05). It is found to be 1.53, 1.087 and 1.024, respectively, while P_c is the cylinder pressure during the injection process. It depends primarily on compression ratio, valve timing and injection timing. Cylinder pressure is modeled mathematically by solving the energy equation as well as the equation of state. Kinematics of piston motion is essential also to assign the instantaneous cylinder volume as follows:

- *Energy equation*

Neglecting heat losses during the compression stroke, energy equation becomes as follows:

$$-P_c \frac{dV_c}{dt} = \frac{dE_c}{dt} \quad (40)$$

where E is the internal energy of charge inside the cylinder during the compression stroke, which is considered as pure air with constant composition. Then, it is calculated as follows:

$$E_c = n_{O2} e_{O2} + n_{N2} e_{N2} \quad (41)$$

- *Equation of state*

$$P_c V_c = n R_u T_c \quad (42)$$

- *Crank slider mechanism*

$$V_c = V_\theta + \frac{V_{st}}{CR-1} \quad (43)$$

and,

$$V_\theta = \frac{\pi}{4} D_p^2 L_{con} \left[(1+\lambda) - \left(\lambda \cos\theta + \sqrt{1-(\lambda \sin\theta)^2} \right) \right] \quad (44)$$

The last set of equations is solved together staring from the closing angle of inlet valve, which is considered as the beginning of compression stroke. Ambient pressure and temperature are considered as initial conditions at this angle. As a result, the instantaneous cylinder pressure with respect to crank rotation angle 'θ' is obtained, which in turn is used to calculate the injection pressure ratio represented in Eq. (39). Figure 21 shows the great dependency of injection pressure ratio on biodiesel blends. This returns to the wide range of variation in their properties. Injection timing shows little effect with neat biodiesel (B100) only. The late injection means relatively higher back pressure, which contributes to diminish the effect of physical properties as in Eq.(39). Results shows also insignificant effect of the injection timing on injection pressure ratio in case of low blends ratios (B20 and B05).

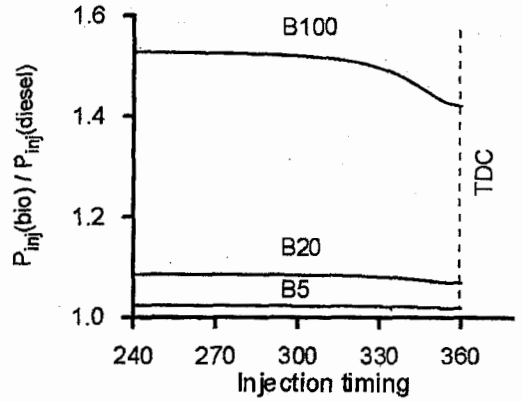

Fig. 21 Effect of blend ratio and injection timing on injection pressure (compression ratio 17 and reference injection pressure 175 bar)

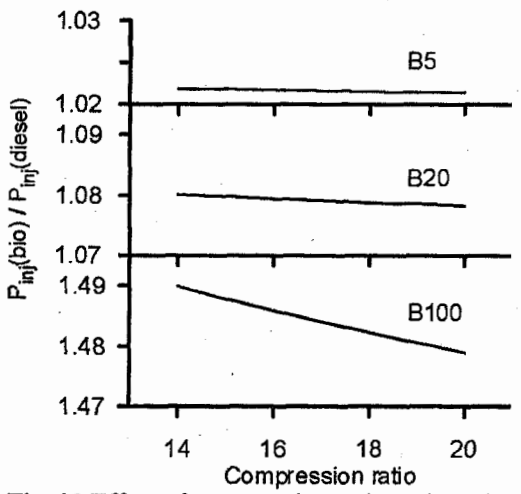

Fig. 22 Effect of compression ratio on injection pressure ratio at different bidiesel blends

It is concluded from previous results that, the fuel properties are the dominant factor affecting spray characteristics and atomization process rather than the operating conditions which exhibit lower influence.

5. CONCLUSION

In the present work, a mathematical model is introduced to emulate the performance of fuel injection system in diesel engines. The model is used to study the behavior of the fuel system when running with biodiesel as a fuel. The results show the following:

- Pressure waves traveling through pipeline are diminished rapidly compared with conventional diesel oil. So the probability of after-injection occurrence is reduced.

- Leakage through the clearance between moving parts decreased in case of using biodiesel as a result of its higher viscosity. Using B20 reduces the leakage just by 6.5 %, while B100 reduces the leakage by 32%.
- Due to the reduction in leakage, and in addition to the higher rate of pressure rise, the quantity of fuel injected per cycle increases with increasing biodiesel blend ratio.
- Injection timing becomes earlier with biodiesel and its blends. Injection starts 1.2 crank angle degrees early relative to B0 (pure diesel fuel) when using B100.
- Slight decrease in residual pressure inside pipeline is obtained when increasing biodiesel blend ratio. This contributes to reducing the probability of after-injection occurrence specially at high loads.
- In spite of poorer properties of biodiesel compared with diesel fuel from atomization point of view, the study indicates that the same level of atomization can be obtained by increasing injection pressure with specified ratios. These ratios depend mainly on the biodiesel blend ratio and engine compression ratio. While injection timing has insignificant effect.
- As a result of earlier opening injector when using biodiesel, it is recommended either to raise the fuel injection pressure which leads to enhancing the atomization process or to delay the injection timing.

NOMENCLATURE

A	Area	m^2
a	Sonic speed	m/s
a_p	Cam follower acceleration	m/s^2
C	Courant number	
C_d	Coefficient of discharge	
D	Distance between base circle and nose circle centers	m
d_p	Plunger diameter	m
d_n	Needle valve diameter	m
E	Bulk modulus	$MPa.$
E_c	Internal energy for cylinder contents during compression	j
e	Specific internal energy for each species	$j/kmol$
k	Spring stiffness	N/m
L_{st}	Effective stroke of pump	m
l	Cam follower lift	m
m	mass	kg
n	Number of moles	
n_h	Number of injection holes	
P	Pressure	$Pa.$
ΔP_L	Difference between line pressure and cylinder pressure during the injection process	$Pa.$
Q_d	Fuel discharged to the delivery chamber	m^3/s
Q_{in}	Fuel inlet flow rate to pump barrel or to needle chamber	m^3/s
Q_{inj}	Fuel injected through nozzle	m^3/s
Q_l	Leakage flow rate	m^3/s
Q_n	Rate of change of displacement volume due to needle motion	m^3/s
Q_{pip}	Fuel delivered to pipe line	m^3/s
R_u	Universal gas constant	$j/kmol.K$
R	Radius of cam follower	m
R_b	Radius of base circle	m
PR	Injection pressure ratio defined in Eq. (38)	
r_n	Nose circle radius	m
u	velocity	m/s
V_c	Instantaneous cylinder volume	m^3
V_d	Volume of delivery chamber	m^3
V_n	Volume of needle chamber	m^3
V_p	Volume inside pump barrel	m^3
x	Instantaneous delivery valve lift or axial flow direction in pipe line	m
x_r	Relief stroke for delivery valve	m
y	Instantaneous needle valve lift	m

Subscript/superscript

d	Delivery valve / chamber
h	Injector hole
in	Inlet port
n	Needle valve
o	Pump inlet condition
p	Plunger
r	Relief stroke
v	Vapor

Greek letters

α	Angle of helical groove in plunger	$degree$
Δ	Clearance between plunger/ needle bush	m
μ	Dynamic viscosity	$Pa.s$
θ	Cam angle	$degree$
ρ	density	kg/m^3
ϕ	Total rise period of cam profile	$degree$
ϖ	Rotational speed	rad/s

ABBRIVIATIONS

ABDC	After bottom dead center
ATDC	After top dead center
BBDC	Before bottom dead center
BTDC	Before top dead center
E.V.C	Exhaust valve closing angle
E.V.O	Exhaust valve opening angle
I.V.C	Inlet valve closing angle
I.V.O	Inlet valve opening angle

6. REFERENCES

[1] Altin R. , Cetinkaya S. and Yucesu H. S. "The Potential of Using Vegetable Oil Fuels as Fuel For Diesel Engines" Energy Conversion and Management Vol. 42, pp. 529-538, 2001.

[2] Bari S., Lim T. H. and Yu C. W. "Effects of Preheating of Crude Palm Oil (CPO) on Injection System, Performance and Emission of A Diesel Engine" Renewable Energy, Vol. 27, pp. 339-351, 2002.

[3] Nwafor O. M. F. "The Effect of Elevated Fuel Inlet Temperature on Performance of Diesel Engine Running on Neat Vegetable Oil at Constant Speed Conditions" Renewable Energy , Vol. 28 ,pp. 171-181, 2003.

[4] Nwafor O. M. F. "Emission Characteristics of Diesel Engine Running on Vegetable Oil With Elevated Fuel Inlet Temperature" Biomass and Bioenergy, Vol. 27 , pp. 507-511, 2004.

[5] Kusdiana D. and Saka S. "Methyl Esterification of Free Fatty Acids of Rapeseed Oil as Treated in Supercritical Methanol" Journal of Chemical Eng. of Japan, Vol. 34, No. 3, pp. 383-387, 2001.

[6] Kato S., Kunisawa K., Kojima T. and Murakami S. "Evaluation of Ozone Treated Fish Waste Oil as A Fuel For Transportation" Journal of Chemical Eng. of Japan, Vol. 37, No. 7, pp. 863-870, 2004.

[7] Shaheed A. and Swain E. "Performance and Exhaust Emission Evaluation of a Small Diesel Engine Fuelled with Coconut Oil Methyl Esters" SAE Technical paper, No. 981156, pp. 1-7, 1998

[8] Machacon H. T. C. , Matsumoto Y. , Ohkawara C. , Shiga S. , Karasawa T. and Nakamura H." The Effect of Coconut Oil and Diesel Fuel Blends on Diesel Engine Performance and Exhaust Emissions" JSAE Review Vol. 22 , pp. 349-355, 2001.

[9] Machacon H. T. C., Shiga S., Karasawa T. and Nakamura H. "Performance and Emission Characteristics of A Diesel Engine Fueled With Coconut Oil-Diesel Fuel Blend" Biomass and Bioenergy, Vol. 20, pp. 63-69, 2001.

[10] M.A. Kalam, Husnawan M. and Masjuki H. H. "Exhaust Emission and Combustion Evaluation of Coconut Oil-Powered Indirect Injection Diesel engine " Renewable Energy, Vol. 28, pp. 2405-2415, 2003.

[11] Ozaktas T. "Compression Ignition Engine Fuel Properties of a Used Sunflower Oil-Diesel Fuel Blend" Energy sources, Vol. 22, pp. 377-382, 2000.

[12] Usta N., Ozturk E., Can O., Conkur E. S., Nas S., Con A. H., Can A. C. and Topcu M. "Combustion of Biodiesel Fuel Produced From Hazelnut Soapstock/Waste Sunflower Oil Mixture in A Diesel Engine" Energy Conversion and Management, Vol. 46, pp. 741-755, 2005.

[13] Silvio C. A. , Belchior C. R. , Nascimento M.V.G. , Vieira L. S. R and Fleury G. "Performance of A Diesel Generator Fuelled With Palm Oil" Fuel, Vol. 81, pp. 2097-2102, 2002.

[14] Nwafor O. M. I. "Emission Characteristics of Diesel Engine Operating on Rapeseed Methyl Ester" Renewable Energy, Vol. 29, pp. 119-129, 2004.

[15] Tsolakis A. and Megaritis A. "Exhaust Gas Assisted Reforming of Rapeseed Methyl Ester For Reduced Exhaust Emissions of CI Engines" Biomass and Bioenergy, Vol. 27, pp. 493-505, 2004.

[16] Lapuerta M. , Armas O. , Ballesteros R. and Fernandez J. "Diesel Emissions From Biofuels Derived From Spanish Potential Vegetable Oils" Fuel, Vol. 84, pp. 773-780, 2005.

[17] Selim M. Y. E. , Radwan M. S. and Elfeky S. M. S. "Combustion of Jojoba Methyl Ester in an Indirect Injection Diesel Engine" Renewable Energy, Vol. 28, pp. 1401-1420, 2003.

[18] Huzayyin A. S. , Bawady A. H. , Rady M. A. and Dawood A. "Experimental Evaluation of Diesel Engine Performance and Emission Using Blends of Jojoba Oil and Diesel Fuel" Energy Conversion and Management, Vol. 45, pp. 2039-2112, 2004.

[19] Forson F. K. , Oduro E. K. and Hammond-Donkoh E. "Performance of Jatropha Oil Blends in A Diesel Engine" Renewable Energy, Vol. 29, pp. 1135-1145, 2004.

[20] Pramanik K. "Properties and Use of Jatropha Curcas Oil and Diesel Fuel Blends in Compression Ignition Engine" Renewable Energy, Vol. 28, pp. 239-248, 2003.

[21] Kumar M. S. , Ramesh A. and Nagalingam B. "An Experimental Comparison of Methods To Use Methanol and Jatropha Oil in A Compression Ignition Engine " Biomass and Bioenergy, Vol. 25, pp. 309-318, 2003.

[22] Raheman H. and Phadatare A. G. "Diesel Engine Emissions and Performance From Blends of Karanja Methyl Ester and Diesel" Biomass and Bioenergy, Vol.27, pp. 393-397, 2004.

[23] Ramadhas A. S. , Jayaraj S. and Muraleedharan C. "Characterization and Effect of Using Rubber Seed Oil as Fuel in The Compression Ignition Engines" Renewable Energy , Vol. 30, pp. 795-803, 2005.

[24] Agarwal A. K., Bijwe J. and Das L. M. "Effect of Biodiesel Utilization of Wear of Vital Parts in Compression Ignition Engine" ASME, J. of Eng. For Gas Turbines and Power, Vol. 125, pp. 604-611, April 2003.

[25] Agarwal A. K., Bijwe J. and Das L. M. "Wear Assessment in a Biodiesel Fueled Compression Ignition Engine" ASME, J. of Eng. for Gas Turbines and Power, Vol. 125, pp. 820-826, July 2003.

[26] Terry B. "Impact of Biodiesel on Fuel System Component Durability" NREL Technical Report, December 2005.

[27] Chang D. Y. Z. and Van Gerpen J. H. "Fuel Properties and Engine Performance For Biodiesel Prepared from Modified Feedstocks" SAE Technical paper, No. 971684, pp. 153-172, 1997.

[28] Serdari A. , Fragioudakis K. , Kalligeros S. , Kalligeros S. and Lois E. "Impact of Using Biodiesels of Different Origin and Additives on the Performance of a Stationary Diesel Engine" ASME, J. of Eng. for Gas Turbines and Power, Vol. 122, pp. 624-631, October 2000.

[29] Agarwal A. K. and Das L. M. "Biodiesel Development and Characterization For Use as a Fuel in Compression Ignition Engines" ASME, J. of Eng. for Gas Turbines and Power, Vol. 123, pp. 440-447, April 2001.

[30] Senda J., Okui N., Tsukamoto T. and Fujimoto H. " On-Board Measurement of Engine Performance and Emissions in Diesel Vehicle Operated with Bio-diesel Fuel" SAE Technical paper No. 2004-01-0083, pp. 1-8, 2004.

[31] Senda J., Okui N., Suzuki T. and Fujimoto H. "Flame Structure and Combustion Characteristics in Diesel Combustion Fueled with Bio-diesel" SAE, Technical paper No. 2004-01-0084, pp. 1-12, 2004.

[32] Miyata I., Takei Y., Tsurutani K. and Okada M. "Effects of Bio-Fuels on Vehicle Performance: Degradation Mechanism Analysis of Bio-Fuels" SAE, Technical paper No. 2004-01-3031, pp. 1-9, 2004.

[33] Zarling D. D., Bickel K. L., Waytulonis R. W. and Sweeney J. R. " Improving Air Quality by Using Biodiesel in Generators" SAE technical paper No. 2004-01-3032, pp. 1-10, 2004.

[34] Carraretto C.,Macor A., Mirandola A., Stoppato A. and Tonon S. " Biodiesel as Alternative Fuel: Experimental Analysis and Energetic Evaluations" Energy, Vol. 29, pp. 2195-2211, 2004.

[35] McCormick R. L. , Tennant C. J. , Hayes R.R. , Black S., Ireland J., McDaniel T., Williams A., Frailey M. and Sharp C. A. "Regulated Emissions From Biodiesel Tested in Heavy-Duty Engines Meeting 2004 Emission Standards" SAE Technical Paper No. 2005-01-2200, pp. 1-11, 2005.

[36] Choi C. Y. , Bower G. R. and Reitz R. D. "Effects of Biodiesel Blended Fuels and Multiple Injections on D. I. Diesel Engines", SAE Technical paper No. 970218, 1997.

[37] Alam M., Song J., Acharya R., Boehman A. and Miller K. " Combustion and Emissions Performance of Low Sulfur, Ultra Low Sulfur and Biodiesel Blends in a DI Diesel Engine" SAE Technical paper No. 2004-01-3024, pp. 1-12, 2004.

[38] Nurun Nabi M., Shahadat M. Z., Rahman M. S. and Rafiqul Alam M. " Behavior of Diesel Combustion and Exhaust Emission with Neat Diesel Fuel and Diesel-Biodiesel Blends" SAE Technical paper No. 2004-01-3034, pp. 1-8, 2004.

[39] Engine Manufacturers Association " Test Specifications For Biodiesel Fuel" EMA report, May 31, 2006.

[40] National Biodiesel Board Guidance , " Use of Biodiesel Blends above 20% Biodiesel" Issued November 30, 2005.

[41] Ahouissoussi N. B. C. and Wetzstein M. E. "A Comparative Cost Analysis of Biodiesel, Compressed Natural Gas, Methanol and Diesel For Transit Bus Systems" Resources and Energy Economics, Vol. 20, pp. 1-15, 1997.

[42] Wilson S. A. " Theoretical and Experimental Investigation of The Fuel Injection System For Diesel Engines" M.Sc., Menoufia University, 1983.

[43] Heldt P. M. "High Speed Combustion Engines" Oxford & IBH Pub. 2nd edition, chapter 14, pp.368-373, 1969.

[44] Heywood J. B. "Internal Combustion Engine Fundamentals" McGraw Hill., international edition, pp. 760, 1988.

[45] Douglas J. F., Gasiorek J. M. and Swaffield G. A. "Fluid Mechanics" Pitman Pub. Ltd, ch. 8 , pp. 243-281, 1981.

[46] Syam A. R. "Untersuchungen zum Einspritz-verlauf bei mittelschnellaufenden Dieselmotoren mit hohen Einspritzdrucken" Doktor-Ingenieur Dissertation, Technischen Universitat "Otto von Guericke" Magdeburg, 1991.

[47] Allen C. A. W., Watts K. C., Ackman R. G. and Pegg M. J. " Predicting The Viscosity of Biodiesel Fuels From Their Fatty Acid Ester Composition" Fuel Vol. 78, pp. 1319-1326, 1999.

[48] Tat M. E. and Van Gerpen J. H. "Physical Properties and Composition Detection of diesel Fuel Blends" *ASAE Meeting Paper Number: 026084, pp.1-11, 2002.*

[49] Tat M. E. and Van Gerpen J. H. "Measurement of Biodiesel Speed of Sound and Its Impact on Injection Timing" NREL/SR-510-31462, Final Report, February 2003.

[50] Shi X., Yu Y., He H., Shuai S., J. Wang J. and Li R. "Emission Characteristics Using Methyl Soyate–Ethanol–Diesel Fuel Blends on A Diesel Engine" Fuel Vol. 84, pp. 1543-1549, 2005.

[51] Ejim C. E. , Fleck B. A. and Amirfazli A. "Analytical Study For Atomization of Biodiesels and Their Blends in A Typical Injector: Surface Tension and Viscosity Effects" Fuel, pp.1-11, 2006.

Appendix A

Effective discharge area for injector

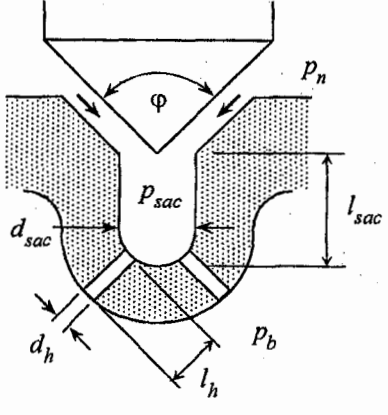

Fig. A1 Nozzle geometry

When needle opens, the fuel flows into tiny container called sac then it injects to the beck pressure through the injection holes. Because of its very small volume, the compressibility effect inside sac is neglected. Effective cross section area for fuel discharged from needle chamber to back pressure is calculated as follows.

$$A_{eff} = \frac{(C_{dn}A_n)(C_{dh}A_h)}{\sqrt{(C_{dn}A_n)^2 + (C_{dh}A_h)^2}} \quad (A.1)$$

where, C_{dn} is the coefficient of discharge through needle valve and A_n is the instantaneous geometrical cross section area between needle cone and its seat. Its value depends on both the needle cone angle φ and its lift as follows.

$$A_n = \pi d_c y \sin\varphi/2 \quad (A.2)$$

Coefficient of discharge through injection holes C_{dh} is calculated as follows [42].

$$C_{dh} = \frac{1}{\sqrt{1.5 + \frac{l_h}{d_h\left(1.14 + 2\log\frac{k}{d_h}\right)^2}}} \quad (A.3)$$

where, k is the absolute roughness for inner surface of the injection holes, which lies in the range of 1 μm. If injection hole has 0.3 mm diameter and 1 mm length, the resultant coefficient of discharge is almost 0.76. The geometrical cross section area of injection holes is.

$$A_h = n_h \frac{\pi}{4} d_h^2 \quad (A.4)$$

where, n_h is the number of injection holes in the nozzle. The sac pressure is then assigned according to the following relation.

$$P_{sac} = \frac{(C_{dn}A_n)^2 P_n + (C_{dh}A_h)^2 P_b}{(C_{dn}A_n)^2 + (C_{dh}A_h)^2} \quad (A.5)$$

Appendix B

Properties of soy bean methyl ester and its blend.

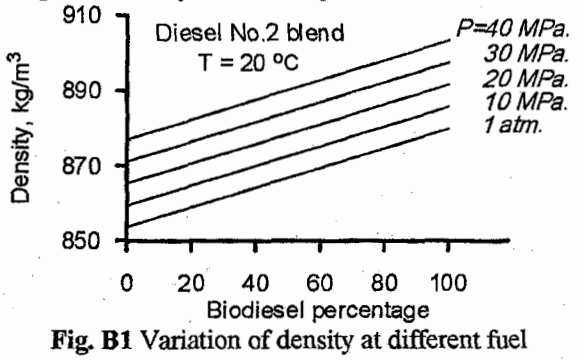

Fig. B1 Variation of density at different fuel pressure

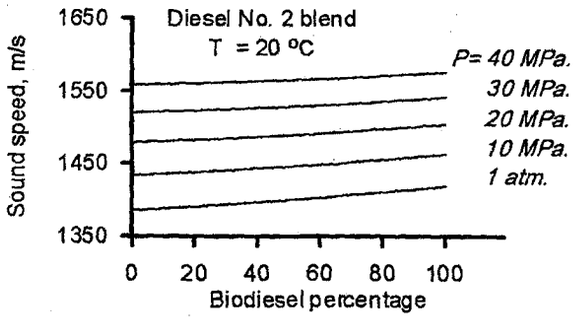

Fig. B2 Speed of sound at different fuel pressure

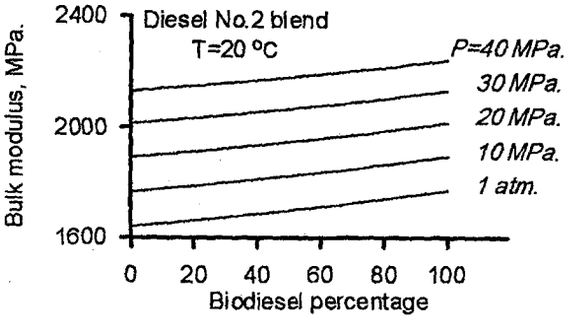

Fig. B3 Bulk modulus at different fuel pressure

Table B.1 Physical and chemical properties of commercial diesel No.2 , No. 1 and biodiesel. [48]

property	No. 2 Diesel	No. 1 Diesel	Soy methyl ester
Carbon (% mass)	86.70	86.83	77.1
Hydrogen (% mass)	12.71	12.72	11.81
Oxygen (% mass)	--	--	10.97
Sulfur (% mass)	0.041	0.045	< 0.005
Cetane number (ASTM D613)	42.6	45.3	51.5
Net HV (kj/kg)	42640	43281	37.388

Appendix C

Technical specifications of Deutez F1L511 engine

Type	DEUTZ F1L511 Four stroke air-cooled
Number of cylinders	Single cylinder
Bore × Stroke	100 mm × 105 *mm*
Cylinder capacity	825 cm^3
Injection angle	24 *BTDC*
Injection pressure	175 *bar*
Compression ratio	17
I.V.O	32° *BTDC*
I.V.C	59° *ABDC*
E.V.O	71° *BBDC*
E.V.C	32° *ATDC*